Korean J. Chem. Eng., **29**(9), 1259-1265 (2012)
DOI: 10.1007/s11814-011-0301-4

Electroless deposition of NiMoP films using alkali-free chemicals for capping layers of copper interconnections

Hae-Min Lee*, Heeyeop Chae, and Chang-Koo Kim*,†**

*Department of Chemical Engineering and Division of Energy Systems Research, Ajou University, Suwon 443-749, Korea
**Department of Chemical Engineering, SungKyunKwan University, Suwon 440-746, Korea
(*Received 4 August 2011 • accepted 21 December 2011*)

Abstract–NiMoP films were electrolessly deposited on copper substrates in a bath containing alkali-free chemicals. The film characteristics such as composition, thickness (or deposition rate), and microstructure were investigated by varying the concentration of the electrolyte. The film thickness increased with nickel ion concentration and decreased with increasing concentrations of either molybdate or hypophosphite ions. The nickel, molybdenum, and phosphorous content of the film increased as the concentrations of their corresponding precursors increased in the bath. Microstructural analysis showed that amorphous films formed when the combined content of molybdenum and phosphorous in the film was sufficiently high. Higher combined contents of molybdenum and phosphorous also improved the corrosion resistance of the film.

Key words: NiMoP Films, Electroless Deposition, Alkali-free Chemicals, Amorphous, Corrosion Resistance

INTRODUCTION

Copper has received much attention as an interconnecting material in microelectronic devices due to its lower bulk resistivity and higher resistance to electromigration than aluminum [1,2]. However, it is known to easily oxidize and diffuse through an oxide film, causing devices to fail [3,4]. Capping or barrier layers have been tested to prevent copper from oxidation and diffusion.

Iron group metals such as iron, cobalt, and nickel are commonly used to prevent the oxidative corrosion of copper surfaces. However, films deposited from such metals alone have many grain boundaries that provide diffusion pathways for copper. The grain boundaries can be stuffed with phosphorous and refractory metals such as molybdenum and tungsten. Capping or barrier layers based on ternary alloys such as CoWP [5-8], CoWB [9], NiWP [10], NiReP [11], and NiMoP [12,13] have been investigated. Among these, nickel-based amorphous films are attractive because of their capping and barrier abilities as well as their good magnetic properties, durability, and corrosion resistance [14].

Nickel-based ternary films have been prepared by wet chemical methods including electrodeposition, electroless plating, non-isothermal deposition, and self-assembled monolayers [10,12,13]. Such films were made in solutions containing alkali-metals chemicals. However, the presence of alkali-metal ions, such as sodium and potassium ions, gives rise to mobile ionic charges [15]. These ions are detrimental because they have high diffusivities in oxide films that affect the reliability of the devices. Therefore, the fabrication of capping or barrier layers in the absence of alkali-containing chemicals is required.

In this work, NiMoP films were prepared using electroless deposition in the absence of alkali-containing chemicals. The effects of each component (Ni, Mo, and P) on the composition, thickness, and microstructure of the electrolessly deposited NiMoP films were investigated. In addition, the effects of molybdenum and phosphorous contents on the corrosion behavior of the films were also investigated.

EXPERIMENTAL

NiMoP films were electrolessly deposited on copper substrates using alkali-free chemicals. Ammonium nickel sulfate hexahydrate ($(NH_4)_2Ni(SO_4)_2 \cdot 7H_2O$), ammonium molybdate ($(NH_4)_2MoO_4$), and ammonium hypophosphite ($(NH_4)H_2PO_2$) were used as the precursors of nickel, molybdenum, and phosphorus, respectively. Dimethylamineborane ($(CH_3)_2NH \cdot BH_3$, DMAB) was used as a reducing agent. Since DMAB is a strong reducing agent, its use does not require the copper substrate to be activated by a catalyst to initiate the deposition. Ammonium citrate ($HOC(CO_2NH_4)(CH_2CO_2NH_4)_2$) was used as a complexing agent to prevent spontaneous metal reduction and precipitation in the solution. Citrate was chosen because it is non-toxic and has brightening, leveling, and buffering actions [16]. The solution was prepared by dissolving the chemicals in deionized water. The concentrations of nickel, molybdenum, and hypophosphite precursors varied from 0.05 to 0.25, 0.005 to 0.025, and 0.05 to 0.25 M, respectively. The concentrations of DMAB and citrate were fixed at 0.2 and 0.15 M, respectively, in all cases. The pH of the solution was adjusted to 8.35±0.01 by tetramethylammonium hydroxide ($(CH_3)_4N(OH)$, TMAH).

Copper substrates were obtained by physical vapor deposition (PVD) of copper onto silicon wafers. Prior to the copper deposition, a thin titanium film (*ca.* 20 nm) was coated onto the silicon wafer to improve the adhesion of copper to silicon. The copper substrate was cut into 1 cm×2 cm rectangles and lacquered to expose 1 cm^2 for the electroless plating of NiMoP films. Before deposition, the substrate was cleaned by nitrogen gas blowing. The deposition

†To whom correspondence should be addressed.
E-mail: changkoo@ajou.ac.kr

was carried out at 60±1 °C for 3 min. The deposition bath was agitated using a magnetic stirrer at 960 rpm. After deposition, the samples were washed with a jet of water and dried by flowing nitrogen gas.

The thicknesses of the films were measured by a surface profiler (Ambios Technology, XP-1). Their compositions were analyzed by X-ray photoelectron spectroscopy (XPS) and energy dispersive X-ray (EDX). Microstructural analysis of the films was made using a high-power X-ray diffractometer (XRD, Rigaku, D/max-2500V/PC) with a Cu K_α incident beam (wavelength, 0.154 nm) that worked at 40 kV and 150 mA. Surface morphologies were examined by field emission scanning electron microscopy (FE-SEM, Hitachi, S-4800). Corrosion behavior of the films was characterized by a computer-controlled potentiostat (VSP-Princeton Applied Research).

RESULTS AND DISCUSSION

1. Mechanism for Electroless Deposition of NiMoP

The electroless deposition of each species of the NiMoP films took place in the presence of reducing agents such as DMAB and hypophosphite through the following mechanisms [17-19]. First, electrons were produced by the oxidation of each reducing agent, DMAB and hypophosphite, according to reactions (1) and (2), respectively.

$$(CH_3)_2HN{\cdot}BH_3+3HOH+OH^- \rightarrow (CH_3)_2HN^++B(OH)_4^-+5H^++6e^- \quad (1)$$

$$H_2PO_2^-+OH^- \rightarrow H_2PO_3^-+\tfrac{1}{2}H_2+e^- \quad (2)$$

These electrons then participated in the reduction of the nickel (Ni^{2+}), molybdate (MoO_4^{2-}), and hypophosphite ($H_2PO_2^-$) ions. The reduction reactions to form elemental nickel and phosphorous were as follows, respectively.

$$Ni^{2+}+2e^- \rightarrow Ni \quad (3)$$

$$H_2PO_2^-+2H^++e^- \rightarrow P+2H_2O \quad (4)$$

MoO_4^{2-} was reduced to elemental molybdenum through two steps illustrated in reactions (5) and (6). MoO_4^{2-} was first reduced to an intermediate, $[NiCitMoO_2]^{2+}$, in the presence of the complexing agent (ammonium citrtate). Here, NiCit represents the nickel-citrate complex. $[NiCitMoO_2]^{2+}$ was then catalyzed by nickel and reduced to elemental molybdenum.

$$MoO_4^{2-}+[NiCit]^++2H_2O+2e^- \rightarrow [NiCitMoO_2]^{2+}+4OH^- \quad (5)$$

$$[NiCitMoO_2]^{2+}+2H_2O+4e^- \rightarrow Mo+[NiCit]^++4OH^- \quad (6)$$

2. Surface Compositional Analysis

The surface composition of the electrolessly deposited NiMoP films was analyzed by using XPS. Fig. 1 shows XPS spectra of the NiMoP film prepared from 0.1 M $(NH_4)_2Ni(SO_4)_2{\cdot}7H_2O$, 0.01 M $(NH_4)_2MoO_4$ and 0.1 M $(NH_4)H_2PO_2$, with 0.2 M DMAB and 0.15 M ammonium citrate. The survey scan (Fig. 1(a)) suggests that the film contained nickel, molybdenum, phosphorous, oxygen. Some

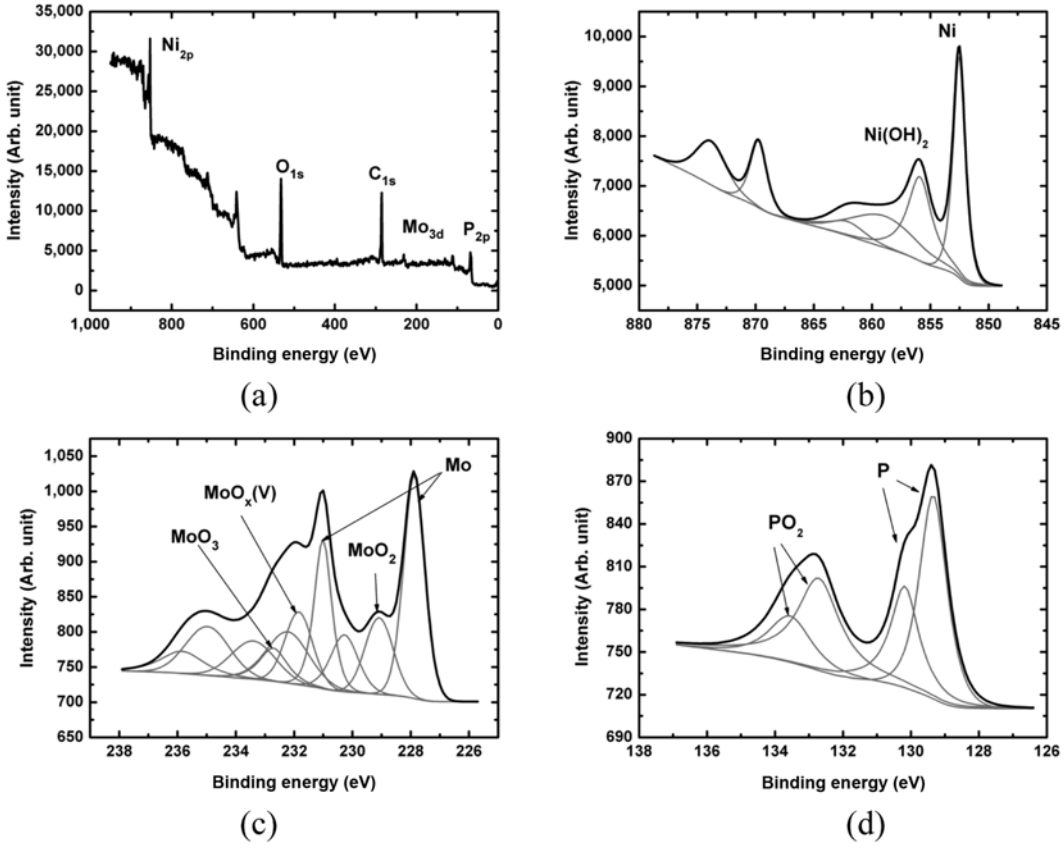

Fig. 1. XPS spectra of NiMoP film electrolessly deposited in a bath containing 0.1 M nickel sulfate, 0.01 M ammonium molybdate, 0.1 M ammonium hypophosphate, 0.2 M DMAB, and 0.15 M ammonium citrate. (a) Survey scan, (b) Ni_{2p}, (c) Mo_{3d}, and (d) P_{2p} electron spectra. Thin gray lines are deconvoluted spectra.

carbon was also detected on the surface of the NiMoP film, possibly due to surface contamination by atmospheric hydrocarbon during storage. The constituent elements (nickel, molybdenum, and phosphorous) were observed in various states.

The Ni 2p spectrum in Fig. 1(b) indicates that nickel existed as elemental nickel and nickel hydroxide, corresponding to the peaks at binding energies of 852.5 and 855.9 eV, respectively [20,21]. The Mo 3d spectrum (Fig. 1(c)) shows four species of molybdenum in the film. The peaks at 227.9 and 231.0 eV correspond to elemental molybdenum and those at 229.1, 231.8, and 232.7 eV indicate the presence of MoO_2, MoO_x (V), and MoO_3, respectively [22-24]. The peaks at 129.3 and 130.2 eV in Fig. 1(d) are due to elemental phosphorous. Those at 132.7 and 133.6 eV are due to PO_2 ions [25,26]. Quantitative analysis by XPS yielded a surface composition of $Ni_{0.64}Mo_{0.1}P_{0.26}$.

3. Effect of Nickel Ion Concentration

Fig. 2 shows the compositions and thicknesses of the electrolessly deposited NiMoP films with respect to nickel ion concentration. The composition was determined by EDX measurements. The concentrations of molybdate and hypophosphite ions were 0.01 and 0.1 M, respectively. Fig. 2(a) shows that the nickel content of the films increased from 67 to 92 at% when the nickel ion concentration rose from 0.05 to 0.25 M. On the other hand, the amounts of both molybdenum and phosphorous in the film concurrently decreased from 13 to 4.3 at% and 20 to 3.7 at%, respectively, with increasing nickel ion concentration. These results suggest that the NiMoP films of this work largely consisted of nickel. Fig. 2(b) shows that the thicknesses of the films increased from 138 to 623 nm with nickel ion concentration, implying that the deposition rate of the film was enhanced by the greater concentration of nickel ions in the solution.

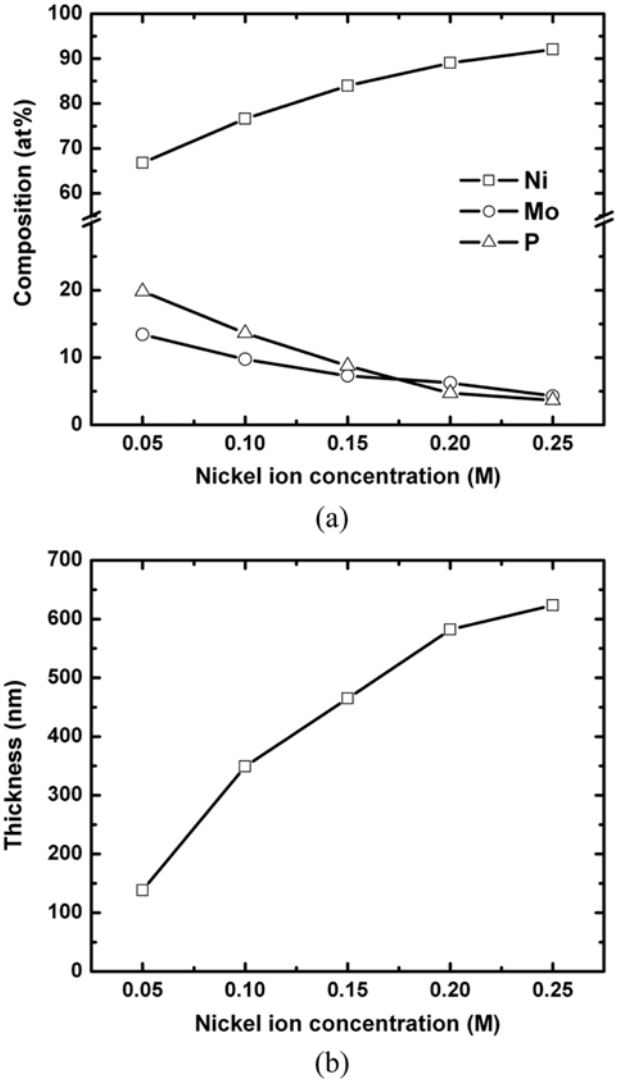

Fig. 2. Effect of nickel ion concentration on (a) composition and (b) thickness of the electrolessly deposited NiMoP films. The concentrations of molybdate and hypophosphite ions were 0.01 and 0.1 M, respectively.

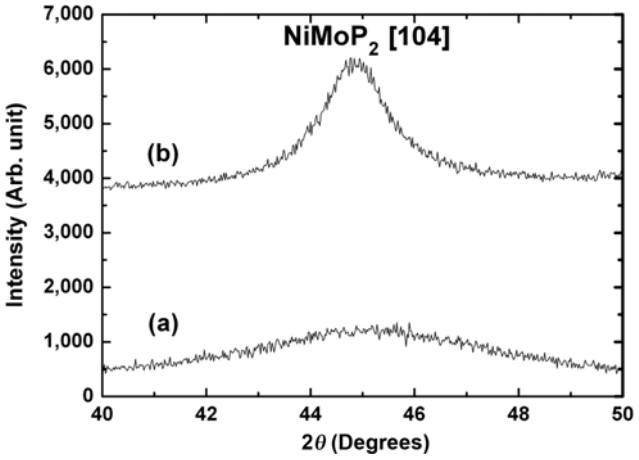

Fig. 3. XRD spectra of NiMoP films electrolessly deposited at nickel ion concentrations of (a) 0.1 M and (b) 0.25 M.

Fig. 3 shows XRD spectra of the NiMoP films electrolessly deposited at nickel ion concentrations of 0.1 and 0.25 M. The film deposited at 0.1 M nickel ion concentration showed no distinct nickel-related peaks, suggesting that it was amorphous. This may be due to the relatively high molybdenum and phosphorous content. Keong et al. [27] reported that high phosphorous content (12-16%) resulted in an amorphous structure electroless Ni-P deposits. Chou et al. [18] revealed that amorphous NiMoP films contained high concentrations of both molybdenum and phosphorous. In the present study, at 0.1 M nickel ion concentration, the molybdenum and phosphorous content in the NiMoP film was 9.8 and 14 at%, respectively. Therefore, the combined content of molybdenum and phosphorous was sufficiently high for amorphous films.

The NiMoP film prepared with a higher concentration of nickel ions (0.25 M) produced a peak at 2θ=44.8° in its XRD spectrum. This corresponds to $NiMoP_2$ [104], implying that the film contained crystallites. It resulted from the lower contents of molybdenum and phosphorous.

Microstructural changes in the NiMoP films with respect to the nickel ion concentration were corroborated by the surface morphologies of the films. Fig. 4 shows SEM images of the NiMoP films deposited at nickel ion concentrations of 0.1 and 0.25 M. The electrolyte with the lower nickel ion concentration produced amorphous NiMoP film with a smooth surface and no crystallites (Fig. 4(a)). The higher nickel ion concentration produced a crystalline NiMoP

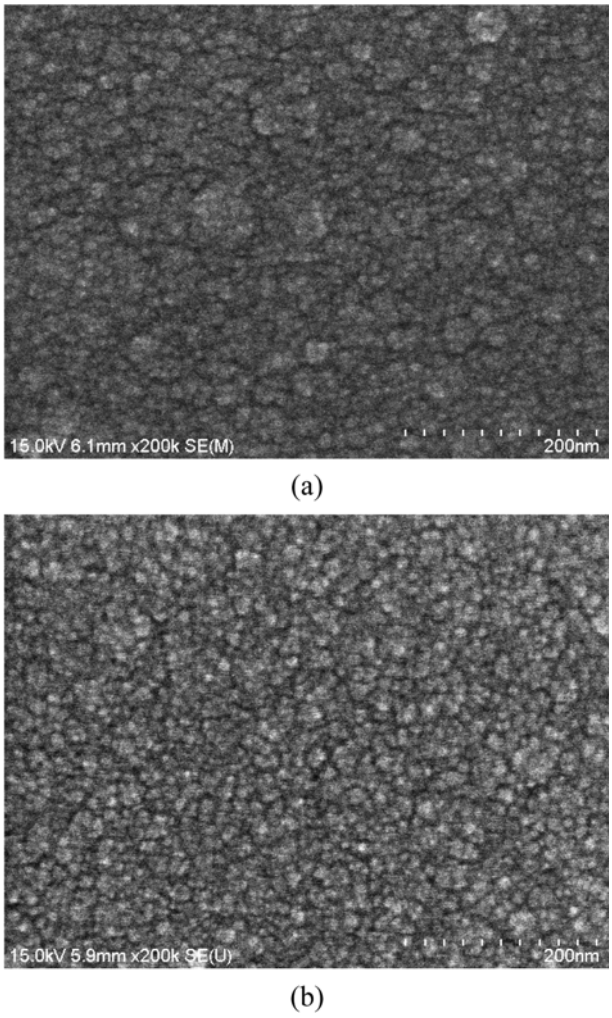

Fig. 4. SEM images of NiMoP films electrolessly deposited at nickel ion concentrations of (a) 0.1 M and (b) 0.25 M.

film with spherical crystallites (Fig. 4(c)).

4. Effect of Molybdenum Ion Concentration

Fig. 5 shows the dependence of composition and thickness of the electrolessly deposited NiMoP films on the molybdate ion concentration. The concentrations of nickel and hypophosphite ions were both 0.1 M. The molybdenum content in the films increased from 4.3 to 15 at% with increasing molybdate ion concentration, while the nickel content decreased from 86 to 76 at%. There was a very little effect of molybdate ion concentration on the phosphorous content of the film. It slightly decreased from 9.8 to 8.3 at% when the molybdate ion concentration was increased from 0.005 to 0.025 M.

Unlike nickel ions, molybdate ions resulted in thinner films with their increased abundance. Film thickness decreased from 612 to 102 nm with increasing molybdate ion concentration (Fig. 5(b)), possibly due to the molybdate ions inhibiting the nickel-based substrate. As stated in section 3.1, molybdate ions were reduced to elemental molybdenum through a two-step mechanism, which includes an intermediate molybdate oxide catalyzed by nickel. During the deposition of NiMoP films, molybdate ions would be adsorbed on the substrate, restricting catalysis by the nickel. Therefore, further molyb-

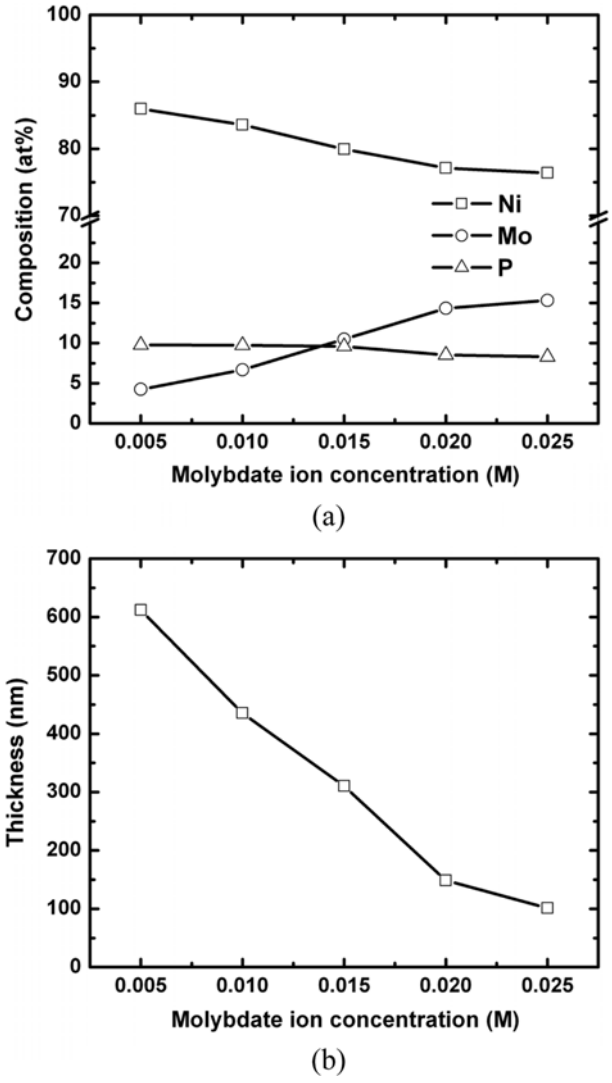

Fig. 5. Effect of molybdate ion concentration on (a) composition and (b) thickness of electrolessly deposited NiMoP films. The concentrations of nickel and hypophosphite ions were both 0.1 M.

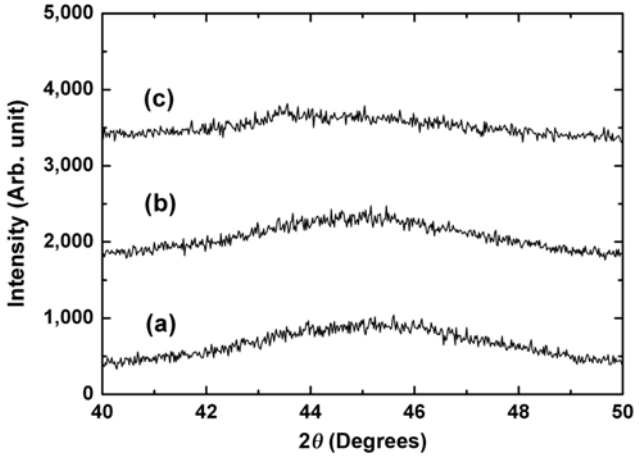

Fig. 6. XRD spectra of NiMoP films electrolessly deposited at molybdate ion concentrations of (a) 0.01 M, (b) 0.015 M, and (c) 0.025 M.

date ions would hinder co-deposition, resulting in a decrease in the thickness of the NiMoP films. This result agrees with other work [18].

Fig. 6 shows XRD spectra of NiMoP films electrolessly deposited at various molybdate ion concentrations. The peaks corresponding to $NiMoP_2$ [104] (2θ=44.8°) are broad and indistinct in all cases, implying that the films were amorphous. This is because the combined content of molybdenum and phosphorous was sufficiently high (>16 at%).

5. Effect of Hypophosphite Ion Concentration

Fig. 7 shows the effect of hypophosphite ion concentration on the composition and thickness of electrolessly deposited NiMoP films. The concentration of nickel and molybdate ions was held at 0.1 and 0.01 M, respectively. The phosphorous content of the films increased from 4.9 to 12 at% as the hypophosphite ion concentration changed from 0.05 to 0.25 M. Concurrent decreases in nickel and molybdenum content were observed: from 92 to 87 at% and from 3.1 to 1.2 at%, respectively. The decrease in nickel content resulted in a decrease in the film thickness with increasing hypophosphite ion concentration, shown in Fig. 7(b).

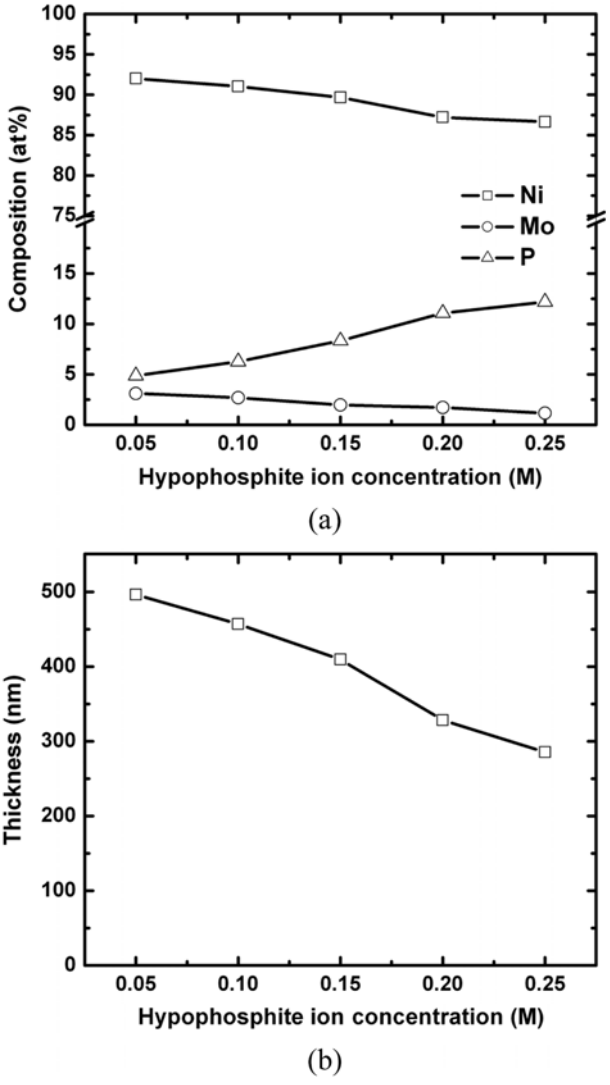

Fig. 7. Effect of hypophosphite ion concentration on (a) composition and (b) thickness of electrolessly deposited NiMoP films. The concentrations of nickel and molybdate ions were 0.1 and 0.01 M, respectively.

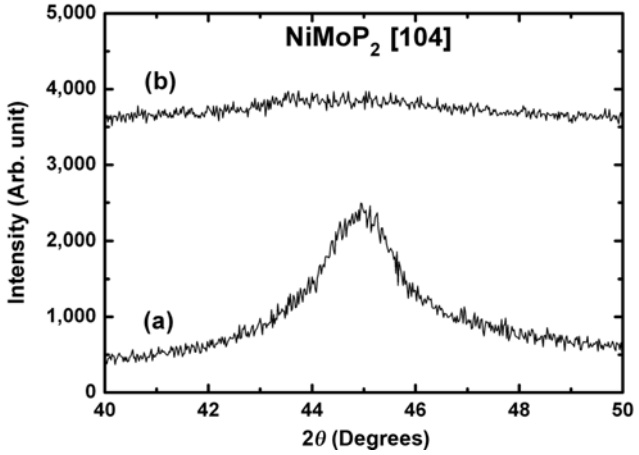

Fig. 8. XRD spectra of NiMoP films electrolessly deposited at hypophosphite ion concentrations of (a) 0.1 M and (b) 0.25 M.

Fig. 8 shows XRD spectra of the NiMoP films electrolessly deposited at hypophosphite ion concentrations of 0.1 and 0.25 M. As the crystallinity of NiMoP film depends on its molybdenum and phosphorous contents, variations of the hypophosphite ion concentration resulted in structural changes. The lower concentration of 0.1 M resulted in molybdenum and phosphorous contents in the NiMoP film of 2.7 and 6.3 at%, respectively. They were not sufficient to stuff the grain boundaries of the NiMoP films. Therefore, a peak corresponding to $NiMoP_2$ [104] is seen in the XRD spectrum. The higher hypophosphite ion concentration of 0.25 M resulted in NiMoP film with no distinct peak corresponding to nickel in the XRD spectrum. This is because the combined content of molybdenum and hypophosphite (*ca.* 15%) was high enough to make the NiMoP film amorphous.

The SEM images of the NiMoP films (Fig. 9) corroborate the microstructural analyses of the NiMoP films at low and high hypophosphite ion concentrations. The film at the lower hypophosphite ion concentration (0.05 M) showed a crystalline structure with spherical crystallites, while an amorphous film was produced at the higher hypophosphite ion concentration (0.25 M).

6. Corrosion Behavior

Previous sections showed that the NiMoP films were amorphous at relatively high combined contents of molybdenum and phosphorous. The molybdenum and phosphorous in such films effectively stuffed the grain boundaries of the films. The addition of molybdenum and phosphorous to Ni-based thin films has been reported to improve their corrosion resistance and thermal stability [28]. To investigate the corrosion behavior of electrolessly deposited NiMoP films at various combined contents of molybdenum and phosphorous, their polarization resistances (corrosion resistances) and corrosion current densities were obtained using polarization curves. Polarization curves of the NiMoP films in a 0.1 M sodium chloride solution were obtained by scanning the potential from −0.10 to −0.65 V at 1 mV/s. The polarization resistance and corrosion current density were then calculated from the polarization curves using the Stern-Geary equation [29].

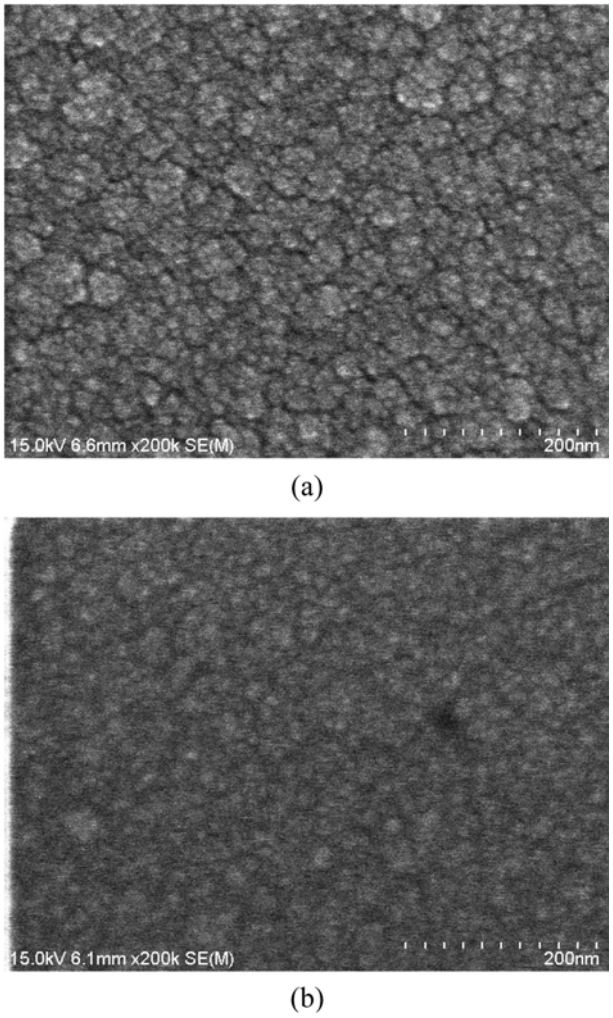

Fig. 9. SEM images of NiMoP films electrolessly deposited at hypophosphite ion concentrations of (a) 0.1 M and (b) 0.25 M.

$$R_p = \frac{\beta_A \beta_C}{2.3(i_{CORR})(\beta_A + \beta_C)} \quad (7)$$

where R_p is the polarization resistance in $k\Omega \cdot cm^2$, i_{CORR} is the corrosion current density in mA/cm^2, and β_A and β_C are the anodic and cathodic Tafel constants, respectively.

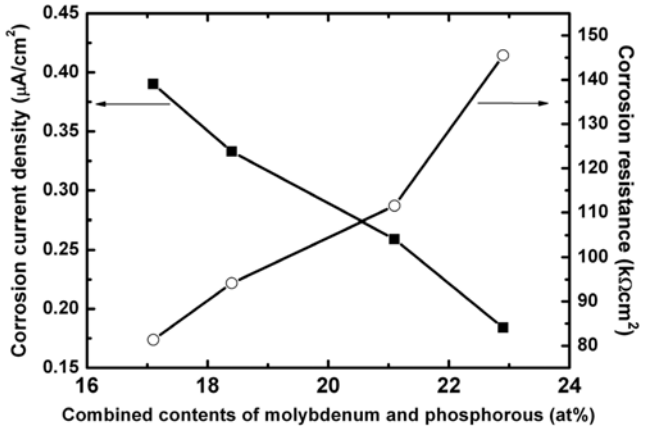

Fig. 10. Effect of the combined content of molybdenum and phosphorous on the corrosion density and polarization resistance of electrolessly deposited NiMoP films.

Fig. 10 shows the polarization resistances and corrosion current densities of NiMoP films with various content of molybdenum and phosphorous. With increased combined content of molybdenum and phosphorous in the NiMoP films, polarization resistances increased and corrosion current densities decreased. Therefore, higher combined contents of molybdenum and phosphorous in the NiMoP films led to better corrosion resistance.

CONCLUSIONS

The electroless deposition of NiMoP films was demonstrated using alkali-free chemicals for their use as capping or barrier layers for copper. XPS analysis showed that the surfaces of the NiMoP films contained elemental nickel, molybdenum, and phosphorous in addition to nickel hydroxide and oxides of molybdenum and phosphorous. With increasing nickel ion concentration, the nickel content and the film thickness (or film deposition rate) increased. Molybdenum and phosphorous content also increased with increasing concentrations of molybdate and hypophosphite ions, respectively. However, the increases in either of these ions led to a decrease in the film thickness. XRD measurements showed that the electrolessly deposited NiMoP films were amorphous when the combined amount of molybdenum and phosphorous in the film was sufficiently high. The combined content of molybdenum and phosphorous also affected the corrosion behavior of the NiMoP films. With increasing combined content of molybdenum and phosphorous in the NiMoP films, polarization resistance increased and corrosion current density decreased.

ACKNOWLEDGEMENT

This work was supported by the Basic Science Research Program through the National Research Foundation of Korea (NRF) funded by the Ministry of Education, Science and Technology (Grant No. 2009-0070734) and an Ajou University Research fellowship of 2010 (Grant No S-2010-G0001-00058).

REFERENCES

1. V. M. Dubin, Y. Shacham-Diamand, B. Zhao, P. K. Vasudev and C. H. Ting, *J. Electrochem. Soc.*, **144**, 898 (1997).
2. P. C. Andricacos, C. Uzoh, J. O. Dukovic, J. Horkans and H. Deligianni, *IBM J. Res. Dev.*, **42**, 567 (1998).
3. Y. Shacham-Diamand, A. Dedhia, D. Hoffstetter and W. G. Oldham, *J. Electrochem. Soc.*, **140**, 2427 (1993).
4. Y. Shacham-Diamand, V. Dubin and M. Angyal, *Thin Solid Films*, **262**, 93 (1995).
5. Y. M. Namkoung, H.-M. Lee, Y.-S. Son, K. Lee and C.-K. Kim, *Korean J. Chem. Eng.*, **27**, 1596 (2010).
6. Y. Shacham-Diamand, Y. Sverdlov and N. Petrov, *J. Electrochem. Soc.*, **148**, C162 (2001).
7. S. M. S. I. Dulal, T. H. Kim, C. B. Shin and C.-K. Kim, *J. Alloy. Compd.*, **461**, 382 (2008).
8. S. M. S. I. Dulal, H. J. Yun, C. B. Shin and C.-K. Kim, *Electrochim. Acta*, **53**, 934 (2007).

9. H. Nakano, T. Itabashi and H. Akahoshi, *J. Electrochem. Soc.*, **152**, C163 (2005).
10. S. B. Antonelli, T. L. Allen, D. C. Johnson and V. M. Dubin, *J. Electrochem. Soc.*, **153**, J46 (2006).
11. T. Osaka, N. Takano, T. Kurokawa and K. Ueno, *Electrochem. Solid State Lett.*, **5**, C7 (2002).
12. Y.-H. Chou, Y. Sung, Y.-M. Liu, N.-W. Pu and M. D. Ger, *Surf. Coat. Technol.*, **203**, 1020 (2009).
13. D.-L. Liu, Z.-G. Yang and C. Zhang, *Mater. Sci. Eng. B*, **166**, 67 (2010).
14. A. Revesz, J. Lendvai, J. Loranth, J. Padar and I. Bakonyi, *J. Electrochem. Soc.*, **148**, C715 (2001).
15. E. B. Deal, *IEEE Trans. Electron. Devices*, **ED-27**, 606 (1980).
16. J. Gambino, J. Wynne, J. Gill, S. Mongeon, D. Meatyard, B. Lee, H. Bamnolker, L. Hall, N. Li, M. Hernandez, P. Little, M. Hamed, I. Ivanov and C. L. Gan, *Microelectron. Eng.*, **83**, 2059 (2006).
17. S. Y. Chang, C. C. Wan, Y. Y. Wang, C. H. Shih, M. H. Tsai, S. L. Shue, C. H. Yu and M. S. Liang, *Thin Solid Films*, **515**, 1107 (2006).
18. Y.-H. Chou, Y. Sung, C.-Y. Bai and M.-D. Ger, *J. Electrochem. Soc.*, **155**, D551 (2008).
19. E. Gomez, E. Pellicer and E. Valles, *J. Electroanal. Chem.*, **580**, 222 (2005).
20. G. K. Wertheim, J. H. Wernick and G. Crecelius, *Phys. Rev. B*, **18**, 875 (1978).
21. J. C. Klein and D. M. Hercules, *J. Catal.*, **82**, 424 (1983).
22. B. Brox and I. Olefjord, *Surf. Interface Anal.*, **13**, 3 (1988).
23. M. Anwar, C. A. Hogarth and R. Bulpett, *J. Mater. Sci.*, **24**, 3087 (1989).
24. Y. Okamoto, T. Imanaka and S. Teranishi, *J. Catal.*, **65**, 448 (1980).
25. M. Taniguchi, S. Suga, M. Seki, H. Sakamoto, H. Kanzaki, Y. Akahama, S. Terada, S. Endo and S. Narita, *Solid State Commu.*, **45**, 59 (1983).
26. C. E. Myers, H. F. Franzen and J. W. Anderegg, *Inorg. Chem.*, **24**, 1822 (1985).
27. K. G. Keong, W. Sha and S. Malinov, *J. Alloy. Compd.*, **334**, 192 (2002).
28. J. Niedbala, *Materials Science Forum*, **514**, 465 (2006).
29. M. Stern and A. L. Geary, *J. Electrochem. Soc.*, **104**, 56 (1957).